A PERFORMANCE COMPARISON STUDY OF GRID-TIED WIND FARM WITHOUT AND WITH BATTERY ENERGY STORAGE SYSTEM

Shankar M
Sri Venkateswara College of Engineering, Sriperumbudur, Tamilnadu, India
shankar.auro@gmail.com

Kumudini Devi R P
College of Engineering Guindy, Anna University, Chennai, Tamilnadu, India
rpkdevi@gmail.com

Abstract: *While integrating the Wind Energy Conversion System to the power grid, power quality issues like power unbalance and harmonic distortion arises. The same can be mitigated by adding battery energy storage system in the DC bus of Class C & D type variable-speed Wind Turbine Generator systems. In simulation studies, the battery energy storage system is represented as a battery bank (direct current sources in series parallel combinations) without considering its actual dynamics. This paper presents a part of the research work that aims at considering the thermodynamics of the battery energy storage by developing a generic model that includes the integration of electrochemical, analytical and electric circuit model approach. To this perspective, a wind farm, AC-DC rectifier, Battery Generic Model, Battery Charge/Discharge Control Logic, DC-AC inverter and open loop radial grid model are developed in PSCAD/EMTDC. Simulations are performed without and with battery energy storage. Mitigation of power quality aspects like power unbalance and harmonic distortion are validated from simulation results. An experimental setup to emulate the power quality issues arising of Class C & D type WTGs and its mitigation using battery energy storage without grid integration is also presented. Vanadium Redox Flow Battery model is used in the simulation study. Both the simulation and emulation results justify power quality issues mitigation with battery energy storage.*

Keywords: *generic battery model, total harmonic distortion, grid integration, wind turbine generator emulator, renewable energy.*

1. Introduction

The increased utilization of power electronics based devices and nonlinear loads exaggerate the distortion of voltage and current waveforms in electrical power system. In addition to the above fact, there is also an increasing trend towards electric deregulation and independent power producers (IIPs) based on renewable energies such as fuel cell, photovoltaic, wind, and gas-fuelled micro-turbines, etc [1]. As like the power quality issues arising of nonlinear loads, renewable energy integration to power grid also challenges power quality issues which is to be dealt with.

This study is constrained to power quality analysis of wind energy conversion systems integrated to power grid. To this context, evaluation of power quality becomes an important issue for the grid integration of wind energy systems [2]. Frequency deviation of power systems caused by grid connected wind power fluctuations is one of the key factors limiting the level of wind penetration. Applying a battery energy storage system (BESS) to overcome the constraint of frequency deviation can increase the level of permitted wind penetration [3, 4]. Also the BEES guarantees that the critical loads are powered when the AC grid fails; in which case, the voltage source inverter (VSI) is controlled as a voltage source. It also accomplishes peak power control by supplying battery power to the local loads while they are powered by the AC grid if the loads get large [5].

For stable frequency control, a BESS is used to generate the nominal system frequency, instead of the synchronous generators. This makes the system frequency independent of the mechanical inertia. In addition, the rapid response of the BESS results in stable operation of the frequency without deviation [6]. The BESS also supports mitigation of voltage unbalance and improves the efficiency of the network [7]. Due to their flexible charging and discharging capabilities, BESS are considered a promising complement to wind farms (WFs) participating in electricity markets [8].

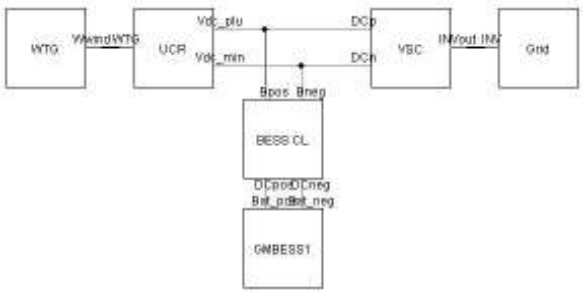

Fig.1. PSCAD/EMTDC model of the proposed methodology; battery bank is represented as a generic model that considers its dynamics at entropy and enthalpy level.

A BESS is characterized by its energy capacity, charge/discharge efficiency, charge/discharge power rate, etc [9]. Within the BESS, there are several technologies which exhibit different behavior which makes them suitable for different grid support services [10]. The applications may be broadly classified as 1) Energy applications: energy time shift, energy arbitrage, peak load management, renewable firming, back-up applications etc. and 2) Power applications: frequency regulation, wind/solar smoothing, ramp support, power quality applications etc. A redox flow battery (RFB) has the capability of having independent control over its energy capacity and power levels by varying its electrolyte and cell stacks respectively. RFB are capable of ensuring a very quick response also [11].

In simulation studies, existing methodologies use the battery model as DC source connected in series-parallel combinations neglecting nonlinear capacity effects [12]. To implement the dynamics of the BESS in the power quality analysis of grid-tied wind farm without and with BESS, a generic battery modeling approach that includes the integration of electrochemical, analytical and electric circuit model approach is adopted in the simulation of proposed methodology. For simulation purpose, vanadium redox flow battery (VRFB) is considered. To this perspective, to analyze the power quality aspects like voltage unbalance and harmonic distortion a wind farm, AC- DC -AC conversion stage, generic battery model, battery switching logic control and grid model are developed in PSCAD/EMTDC.

Section 2 presents the block diagram representation of existing methodology with BESS and the proposed methodology with generic battery model for BESS. Section 3 discusses the development of wind farm model. Section 4 presents the design and development of AC-DC-AC conversion stage. Section 5 describes the generic modeling of BESS and extends its application to model the VRFB ESS. This chapter also justifies the use of VRFB ESS for wind power applications. Section 6 briefs the grid model. Section 7 analyses and compares the simulation results of entire system without and with VRFB ESS and justifies mitigation of power quality issues like voltage unbalance and total harmonic distortion (THD) reduction with VRFB ESS for wind variations and grid side fault conditions [13]. Section 8 presents the experimental setup and justifies THD reduction with BESS integration in wind energy conversion systems (WECS) without grid connection. Section 9 concludes the paper.

Determining the optimal location and size of BESS in a power system network integrated with uncertain wind power generation is also required [14]. Over voltages during high renewable generation periods can be prevented by the locally controlled BESS at the renewable system grid interface [15]. Such a method is adopted in the simulation of proposed methodology. One large VRFB ESS plant can be installed in the potential 'Wind Farms System Center' and the resource of that VRFB ESS can be utilized by all the wind farms by sequentially switching the cell stacks and varying electrolyte volume for power and energy sharing to mitigate power quality issues. Such a system is proposed as future scope of study.

2. Existing and proposed methodology

While analyzing the power quality aspects arising of WECS integrated to grid and its mitigation using BESS, existing methodologies use the battery model as simple DC sources connected in series-parallel combinations neglecting their nonlinear capacity effects. In the proposed methodology, a generic modeling approach for BESS that integrates the electrochemical model at entropy and enthalpy levels enables study of BESS thermodynamics effects over electrical characteristics. The thermodynamical data read from look-up tables into the enthalpy and entropy blocks are varied intentionally and the simulation results are presented to illustrate the percentage of boost and dip in battery voltage during charge and discharge process. The BESS analytical model incorporates the state-of-charge (SOC) dynamic updating equations. Finally the electric circuit model establishes the electrical properties. The BESS generic model is used with a wind farm

integrated to radial power system. The performance analysis of this model for variable wind speed and grid conditions is performed using PSCAD/EMTDC for three cases: 1) without BESS, 2) with generic battery model based BESS without considering the thermodynamics effects of BESS and 3) with generic battery model based BESS considering the thermodynamics effects of BESS. The PSCAD/EMTDC simulation block diagram of the proposed methodology is shown in Figure 1.

3. Wind farm modeling

Wind farms are areas of landscape in potential wind terrain comprising more than one to any number of wind turbine generator units to generate wind power. These areas have the benefit of continuous steady wind speed in the range of 6 m/s to 30 m/s [16]. The wind speeds of 13 m/s is considered annual average and is also best suitable. For any MVA power generation from a permanent magnet synchronous generator directly connected to the wind turbine, the turbine power should be 20% more than generator power to compensate for the friction in the mechanical cycle [17]. For a 3MVA rated PMSG, the wind turbine capacity (S_{turb}) is:

$$S_{turb} = 1.2 \times 3 = 3.6MVA \quad (1)$$

The power coefficient (C_p) for standard wind turbine model in PSCAD/EMTDC is characterized by:

$$C_p = 0.5(\gamma - 0.022\beta^2 - 5.6)e^{-0.17\gamma} \quad (2)$$

where $\gamma = 2.237 \times \frac{wind\ speed}{hub\ speed}$

$\beta = incidence\ angle\ of\ the\ blade$

C_p is maximum at $\beta = 0$. The curve $C_p(\gamma)$ with $\beta = 0$ is shown in Figure 2.

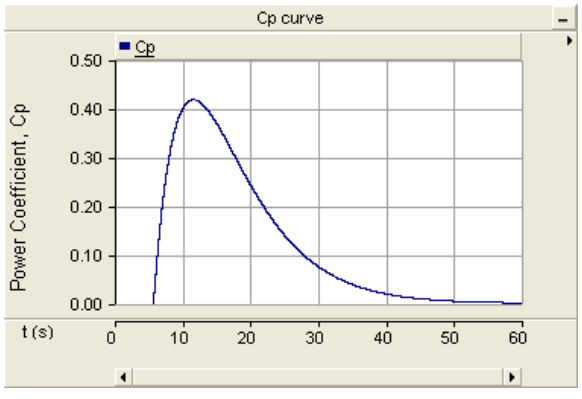

Fig.2. Plot of $C_p(\gamma)$ with $\beta = 0$

Table 1 Wind turbine parameters

Description	Parameters
Rated MVA of turbine	3.6 MVA
Rated angular mechanical speed	3.142 rad/s
Rotor radius	6715.565 m^2
Rotor area	46.234 m
Air density	1.225 kg/m^3

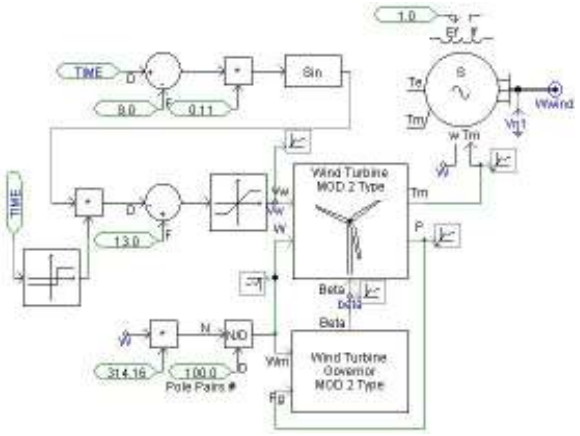

Fig.3. Wind farm model

The turbine rotor radius (R) and area (A) are calculated from the standard power relation:

$$P = \frac{1}{2}\rho A v^3 C_p \quad (3)$$

To model the PMSG with classical synchronous model available with PSCAD/EMTDC, the machine field excitation is held constant (1 per unit). The unsaturated transient time is assumed to be large and unsaturated sub-transient time is assumed to be very small. The permanent magnet synchronous generator parameters are given in Table 1.

A wind farm model comprising one hundred 3 MVA wind turbine generators connected in parallel compounding to total apparent power of 300 MVA is developed by enabling the machine scaling factor in the synchronous generator's parameterization and making the number of coherent machines value to be 100 in the basic data.

The wind source is a variable wind source. For simulation, the wind speed is assumed 13 m/s constant up to 9 s; it starts decreasing and is 4 m/s constant from 16 s to 31 s. Then it starts increasing and is 25 m/s from 48 s to 55 s. It again decreases to reach 8 m/s at the end of simulation. The wind variation is simulated to follow sine function. Dynamic pitch control is established by wind turbine governor component. The complete model is shown in Figure 3.

4. AC-DC-AC conversion stage

In most practical applications, the permanent magnet synchronous generator is directly coupled to the wind turbine with no gear box and gear ratio arrangements as the model developed described in previous chapter. The wind is variable in nature and hence the synchronous generator output frequency varies with variations in wind speed. Considerable drop in frequency leads to increased magnetizing currents in induction machines [18]. So a need arises and necessitates regulation of grid frequency. In these contexts, in order to integrate the variable wind power to the power grid, an AC-DC-AC converter stage is required.

The AC-DC power conversion stage is implemented with a 3-phase diode rectifier. In this study, this stage is parameterized as a 6-pulse bridge with input alpha order set to zero throughout the simulation period. The HV DC control systems are modeled to constrain the DC node voltage to its rated level with a tolerance of +/- 10%. The AC-DC conversion stage is shown in Figure 4.

The DC-AC conversion stage is implemented with 6-pulse GTO voltage inverter. The output of this stage is connected to the power grid through transformer. Two points are to be satisfied at the wind power generation and power grid integration point: 1) the voltage regulation must be effectuated directly at the integration point and 2) the frequency of the inverter must be locked to the grid frequency which can be effectuated by using a phase lock loop (PLL). The voltage regulation at the connection point is achieved by pulse width modulation (PWM) drive. The DC-AC conversion stage is shown in Figure 5.

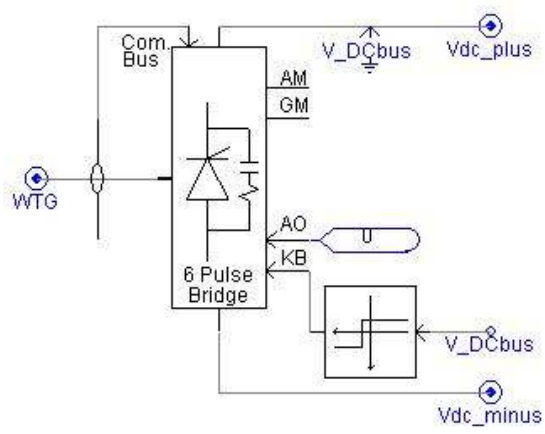

Fig.4. AC-DC conversion stage

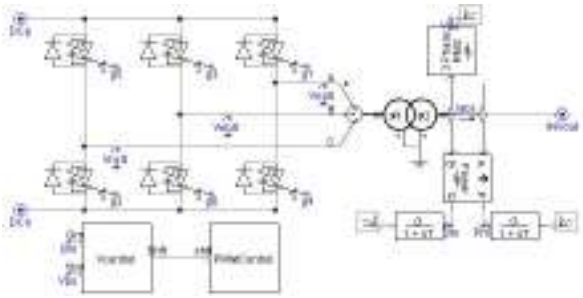

Fig.5. DC-AC inversion stage

5. Generic model of BESS

The battery models presented in literatures including the various advanced electrical models suffer problems during describing their voltage-current characteristics [19]. The voltage-current characteristics exhibited by a battery model should be faithful, and then only it is possible to simulate and study a power system incorporating BESS. Research is in progress to build BESS models that will incorporate their true characteristics. There are models which describe the physical procedures happening in the BESS. Practical models describe the battery behavior in terms of experimental data fitted into governing equations. The theoretical oriented models present the BESS as discrete-time equivalents, electrical circuits, stochastic process models, and so on. Most prefer the combination of various models that offer fitting empirical parameters and simple physical processes [20].

To this context, a generic modeling for BESS that incorporates the entropy and enthalpy blocks which considers the physical process occurring in the battery that outputs the standard reduction potential taking into account the thermodynamic data is proposed. The relation for the same can be arrived from the electrochemistry of batteries.

In this proposed work, the concern is about the battery potential stability for utility shaping and charge-discharge changeover time to address the power quality issues. The kinetic battery modeling approach, which uses the chemical kinetic process as its basics, is adopted in the developing the generic battery model. It uses the state-of-charge (SOC) of battery at every instant of simulation [21, 22]. A SOC-based battery management system (BMS) can control the battery at both grid-connected and islanding operation conditions [23]. Since this work is constrained to study of feasibility of VRFB ESS for wind power applications, the relations and generic modeling pertaining to VRFB ESS is briefed.

The standard reduction potential (E^o) for VRB ESS is given by [24, 25]:

$$E^o = -\frac{\Delta G^o}{nF} = -\frac{\Delta H_r^o - T\Delta S_r^o}{nF}[V] \qquad (4)$$

where ΔH_r^o is standard reaction enthalpy, ΔS_r^o is standard reaction entropy, 'n' the total number of moles transferred during the reaction, F the Faraday constant, $96,485 C/mol$ and T the absolute temperature, $298.15K$.

A generic battery model is developed to generate standard reduction potential for any given battery type by having the thermodynamic data for all battery types in lookup table. Figure 6 shows the model and Figure 7 shows the standard reduction potential plot which is $E^o = 1.23V \, at \, 25^o C$ for VRB ESS. For conditions other than standard, E^o varies.

In the electrical circuit modeling of the BESS, the parameters such as battery potential accounted from the standard reduction potential, internal resistance and its temperature dependence, equivalent capacitance and voltage versus SOC look-up table are to be incorporated [26].

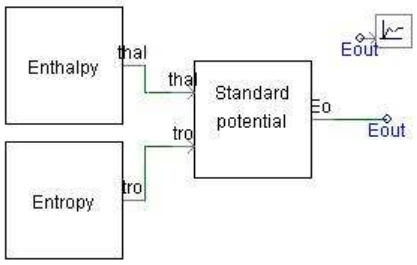

Fig.6. Model that generates the standard reduction potential from thermodynamic data read from look-up table.

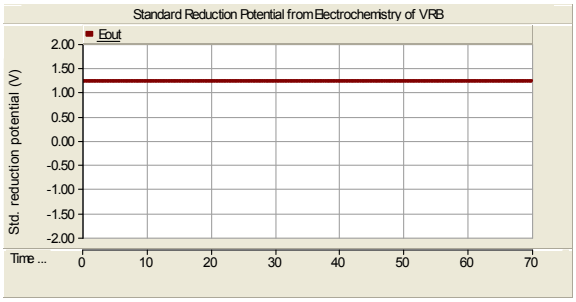

Fig.7. Plot of standard reduction potential which is $E^o = 1.23V \, at \, 25^o C$

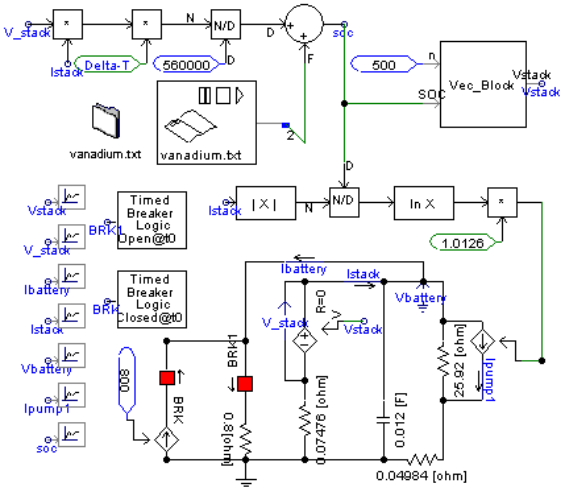

Fig.8. Model of VRB

The electrical circuit model of VRFB ESS is shown in Figure 8. The related parameters are given in Table 2. For VRFB ESS, stack voltage [27] is given by:

$$E_s = n1.\left(E^o + 0.0592 \log\left(\frac{SOC}{1-SOC}\right)\right) \qquad (5)$$

In this model, the rated current of the VRB model is assumed 800A. The VRB is charged with its rated current 800 A for 60 seconds and is discharged at its rated current, -800 A for subsequent 60 seconds. From the simulation results, it is evident that the VRFB output voltage takes 6 ms (59.999s – 60.005s = 0.006s) in reaching steady state. The inertia constant is usually in terms of 'seconds' for a wind turbine. This inherent physical capability facilitates filtering fluctuations in wind power of higher order. Therefore the VRB response time is sufficient for the wind power application. Figure 9 illustrates the simulation of charge to discharge changeover characteristics.

Table 3 presents the comparison of VRB electrical characteristics for variations in thermodynamics. For case (a) the percentage boost in battery voltage during charge (SoC=90%) is 9%. For case (b) the percentage boost in battery voltage during charge (SoC=90%) is 8%. As the thermodynamics worsens, it reflects on electrical characteristics of the battery.

Table 2 Characteristics of VRFB [27]

'$n1$'	R_{fixed}	R_{react}	R_{resist}	$C_{electrode}$
500	25.92Ω	0.07476Ω	0.04984Ω	0.12F

Table 3 Comparison of VRB electrical Characteristics for variations in thermodynamics

Thermodynamics	Process-charge/discharge	Electrical characteristics (V)		
	SOC	30%	90%	30%
$E^0 = 1.386V$	Zero current	670	747	670
	Rated current	729	807	667
$E^0 = 1.236V$	Zero current	594	672	594
	Rated current	654	731	598

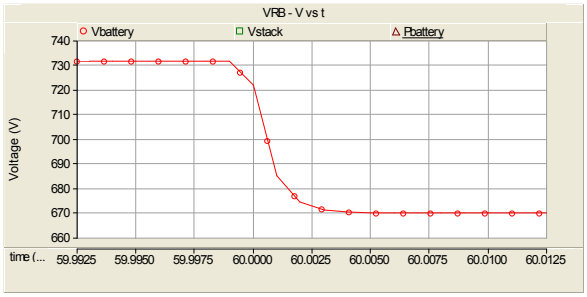

Fig.9. VRB charge (800 A), until 60s and discharge (0.8Ω), for next consequent 60s, output voltage takes 6ms to reach the steady state.

6. Utility grid model

Figure 10 shows the grid model. The grid is modeled as an open loop radial system with loads and source connected as given in Table 4. The wind power is integrated at node-2 through PWM inverter and the simulations are performed to study the voltage unbalance and harmonic distortion effects without and with BESS. The simulation results presented here are for the 3.8MW WECS integrated at node-2. For performance comparison analysis, during simulation, the output of the WECS is opened intentionally from 45s to 50s. Similarly, the load at node-2 is removed from 50s to 55s. Additionally, an equal amount of load already existing at node-2 is added from 60s to 65s to study the voltage unbalance and harmonic distortion effects without and with BESS.

Table 4 Voltage source and load details in grid model

Description	Details
Voltage source	300MVA, 34.5KV, 50Hz
Load @ node-1	(2.133+j1.6) MW
Load @ node-2	(0.266+j0.2) MW
Load @ node-3	(0.266+j0.2) MW
Line impedances between nodes	(1+j5.03)Ω

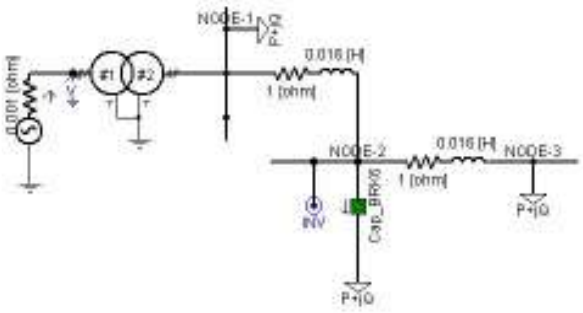

Fig.10. Utility grid model

7. Simulation results and discussions

The node-2 voltage without wind power integration is 0.94pu. When the WECS is integrated at node-2, the node-2 voltage is maintained at 1pu with the WTG supplying 3.6MW. Figure 11 shows the plot of node voltages, THD and power flows in various nodes. Without BESS the variations in the node voltages and power flow at grid integration are significant. The power flow and node voltage variation are in the band 0.013pu and 0.03pu respectively.

Figure 12 shows the same plots with BESS and the effect of thermodynamics intentionally included. The variations in the node voltages and power flow at grid integration are comparably reduced. The power flow and node voltage variation are in the band 0.008pu and 0.001pu respectively.

Figure 13 shows the same plots with BESS and the effect of thermodynamics addressed. The variations in the node voltages and power flow at grid integration are further reduced comparably. The power flow and node voltage variation are in the band 0.006pu and 0.044pu respectively.

Table 5 presents the quantitative analysis of performance indices. The individual harmonics plot is shown in Figure 14. Table 6 presents the measure of individual harmonics and THD at node-2, phase-2. Figure 15 presents the plot of THD at node-2, phase-2.

Table 5 Quantitative analysis of performance indices

Performance indices	Magnitudes in PU		
	Without BESS	With BESS WEoT	With BESS WoEoT
Node-2 power flow variation	0.032-0.045	0.036-0.044	0.039-0.045
Node-2 voltage variation	0.976-1.006	0.988-0.989	0.961-1.005

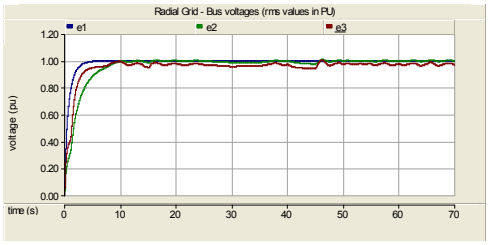

(a)

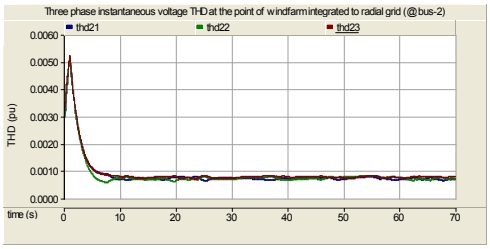

(b)

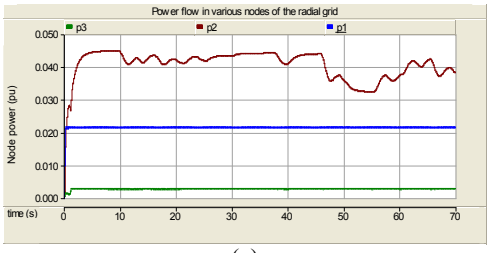

(c)

Fig.11. Plots of performance parameters without battery energy storage system - (a) Node voltages in PU, (b) voltage THD at the node of wind power integration and (c) power flow (pu) in various nodes of grid.

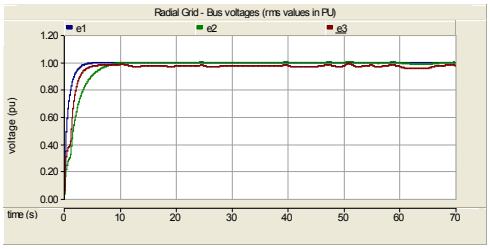

(a)

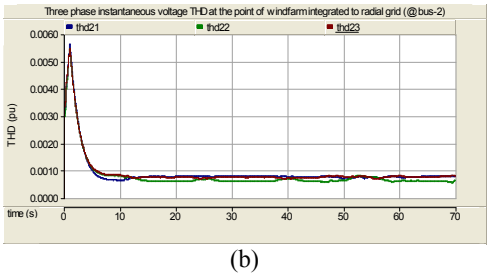

(b)

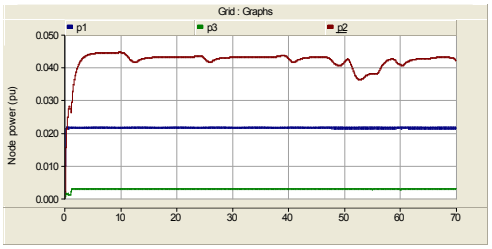

(c)

Fig.12. Plots of performance parameters with battery energy storage system with the effect of thermodynamics (E^0=1.386V) - (a) Node voltages in PU, (b) voltage THD at the node of wind power integration and (c) power flow (pu) in various nodes of grid.

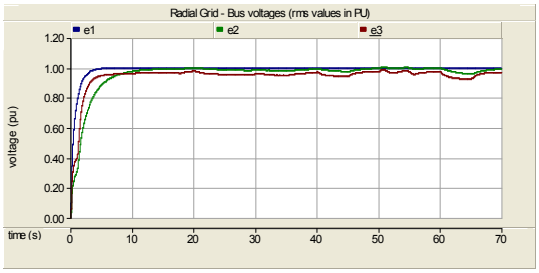

(a)

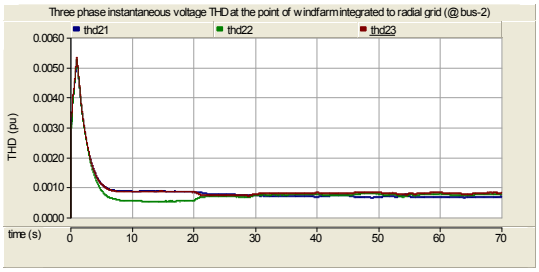

(b)

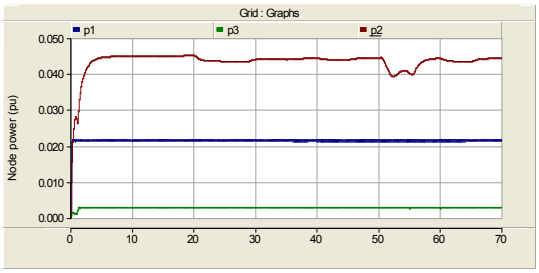

(c)

Fig.13. Plots of performance parameters with battery energy storage system without the effect of thermodynamics (E^0=1.236V) - (a) Node voltages in PU, (b) voltage THD at the node of wind power integration and (c) power flow (pu) in various nodes of grid.

Table 6 Measure of individual harmonics and THD at node-2, phase-2

Harmonic order (h)	Individual harmonics magnitude at node-2 where WTG is integrated		
	Without BESS	With BESS (WEoT)	With BESS (WoEoT)
1	0.984	0.988	0.99
3	0.009	0.007	0.01
5	0.033	0.032	0.03
7	0.012	0.031	0.005
9	0.022	0.016	0.02
11	0.005	0.007	0.01
13	0.022	0.026	0.02
15	0.014	0.028	0.004
THD	**0.052**	**0.062**	**0.044**

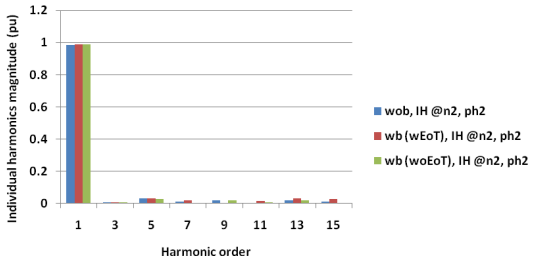

Fig.14. Plot of individual harmonics measured at node-2 where wind power is integrated to grid, without and with battery energy storage system.

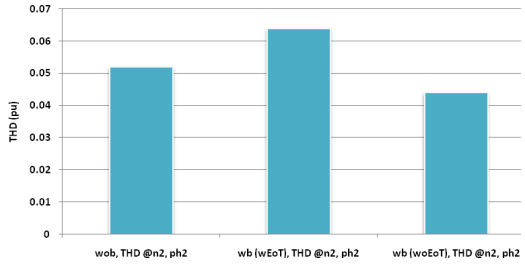

Fig.15. Plot of phase-2 voltage THD at node-2 (PCC)

With BESS and effect of thermodynamics intentionally varied, the THD is comparably increased. Without BESS, the THD is 0.052pu, with BESS and effect of thermodynamics intentionally varied, the THD is 0.062 and with BESS and effect of thermodynamics addressed, the THD is 0.044pu, which is within the standards prescribed by Indian Wind Grid Code [28].

8. Experimental setup

To study the power quality issues arising of variable speed wind turbine generator a practical module is developed. The actual module developed in the laboratory is shown in Figure 16.

DC motor with microcontroller based speed controller is coupled to the 3-phase alternator to emulate variable speed wind turbine generator. The specifications of the wind turbine generator emulator model are given in Table 7. The magnitude of the DC voltage applied to the armature of DC motor is varied through microcontroller coding by varying the duty ratio of the pulses applied to trigger IGBTs of the controlled converter module. Hence variable wind speed is emulated. The cut-in and cut-off wind speeds can be emulated with such an arrangement. By varying the duty ratio of the IGBT connected in the field circuit of the 3-phase alternator, the output voltage of the 3-phase alternator can be varied from potential induced due to residual magnetism to 440V L-L. To emulate permanent magnet synchronous generator (PMSG), the excitation voltage is fixed to a certain value, for study purpose, the duty ratio is fixed at 26% to get an output voltage of 189V L-L.

The output of the alternator is rectified using a 3-phase fully controlled bridge rectifier to get DC output. The specification of the converter is given in Table 8. The output of the converter is fixed at 150V DC by varying the duty ratio of the pulses applied to trigger the SCRs of rectifier.

Table 7 Specifications of WTG emulator model

Wind turbine generator emulator model		
DC motor (1 HP)		
Parameters	***Armature***	***Field***
Voltage	180 V	220V
Current	5.1 A	0.3 A
Speed	1500 rpm	
3-phase alternator (375 VA)		
Parameters	***Stator***	***Rotor (Field)***
Voltage	415 V	220 V
Current	0.52 A	0.4 A
Speed		1500 rpm
Winding connection	Star	
Frequency	50 Hz	
Poles		4

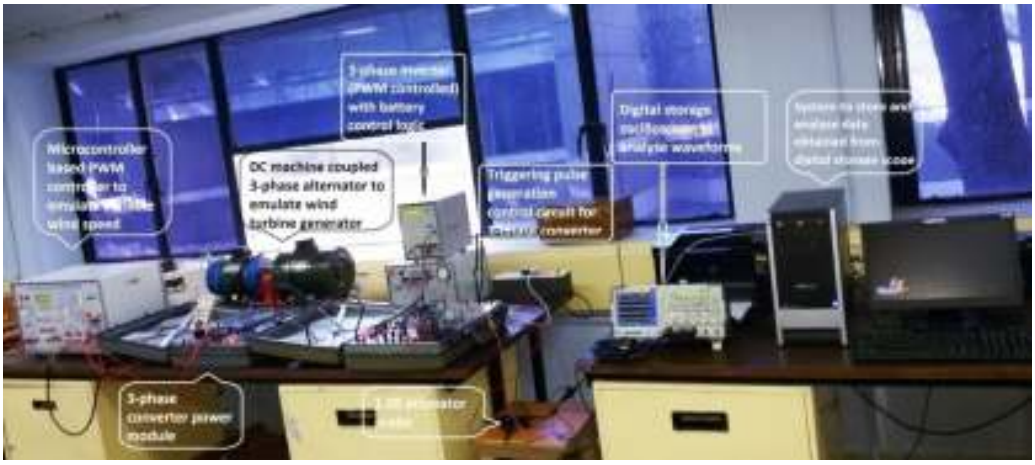

Fig.16. Experimental module developed in the laboratory to emulate variable speed WTG to analyze power quality issues

Table 8 Specifications of 3-phase fully controlled rectifier module

3-phase full controlled converter	
Input	3-phase, 4-wire up to 440V L-L maximum
Output	Up to 550V DC at maximum input voltage of 440V L-L at 15A maximum
Switching device	6 Numbers 25 RIA 120 SCRs, I_{FAV} = 25A, V_{RRM} = 1200V

Table 9 Specifications of DC to 3-phase AC inverter module

DC to 3-phaseAC inverter	
Input	Up to 300V, 2 A DC
Output	3-phase, 4-wire up to 440V L-L
Switching device	6 Numbers IGBT
Control	Microcontroller based PWM pulses, 120 degree conduction mode

An IGBT based DC to 3-phase AC inverter inverts the DC output of the rectifier to 3-phase AC. A microcontroller based pulse width modulation (PWM) generator generates the triggering pulses to trigger the IGBTs in the power module. The without and with battery options are emulated by an UPS mode option in the inverter module. The specification of 3-phase inverter module is given Table 9.

To integrate this complete model to the grid needs special permission obtained from the regional state government authorities. Hence analysis is performed with a star connected load only. Three 18W lamps connected in star emulates load for study purpose. The phase voltages of the inverter output are analyzed using digital storage oscilloscope. The experimental result analysis is presented in the following sub-section.

8.1 Experimental results analysis

Figure 17 (a) shows the frequency excursions due to variable speed operation of WTG due to variations in wind speed which is emulated using a microcontroller based DC motor drive coupled to the synchronous alternator. With a duty ratio of 79% for the pulses applied to trigger the IGBTs in the armature circuit of the DC motor, the speed of the machine is 1255 rpm with the frequency of 3-phase supply from alternator being 42 Hz. When the duty ratio is increased to 83%, the speed of the machine increased to 1507 rpm with the frequency of 3-phase supply from alternator being 50.2 Hz. The excitation voltage of the alternator is varied by varying the duty ratio of pulses applied to trigger the IGBT in the field circuit of the alternator. As discussed earlier, duty ratio is fixed at 26% to get 189V L-L from the alternator.

To analyze the power quality aspects, the DC bus voltage is fixed at 150V DC and is given as input the inverter. The DC to 3-phase inverter is operated in 120 degree conduction mode with PWM switching. Figure 17 (b) shows the output waveform of the inverter observed by digital storage oscilloscope across the phases of star connected load with a 1:20 attenuation probe. The voltage waveform is distorted and, Figure 18 (a), (b), and (c) depicts the THD

spectrum captured by DSO of phase-A, phase-B and phase-C voltages respectively, without ESS in the system.

During cut-in or cut-off wind speeds and transmission line congestions, the WTG output are sufficed by the BESS. This process is emulated by operating the inverter in UPS mode (for experimental purpose). Now the input to the inverter is from the BESS. Again the DC to 3-phase inverter is operated in 120 degree conduction mode with PWM switching. Figure 17 (c) shows the output waveform of the inverter observed through DSO across the phases of star connected load. The voltage waveform is less distorted and, figures 19 (a), (b), and (c) depicts the THD spectrum captured by DSO of phase-A, phase-B and phase-C voltages respectively, with BESS in the system.

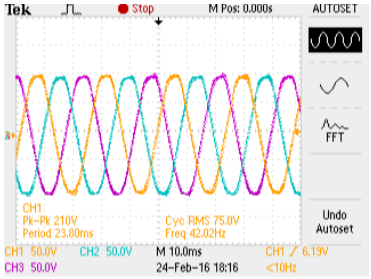

(a)

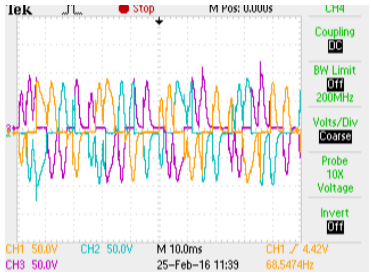

(b)

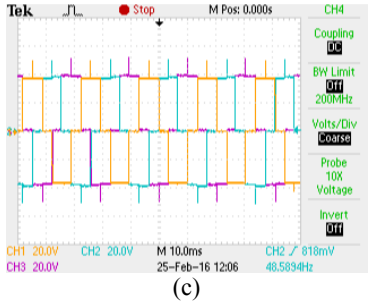

(c)

Fig.17. Emulation results (a) for variable wind speed (1260 rpm, 42Hz), 3-phase alternator output (b) output voltage of the inverter across the load without BESS (c) output voltage of the inverter across the load with BESS.

The harmonic analysis performed using DSO for the three phase voltages without and with battery justifies that without BESS, the THD is more as compared to the system with BESS. With BESS the THD has significantly reduced by 28%.

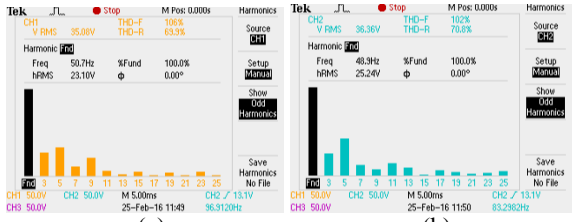

(a) (b)

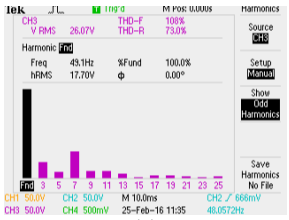

(c)

Fig.18. THD spectrum captured by digital storage oscilloscope (DSO) of phase voltages (a) phase-A, (b) phase-B and (c) phase-C, without BESS in the system.

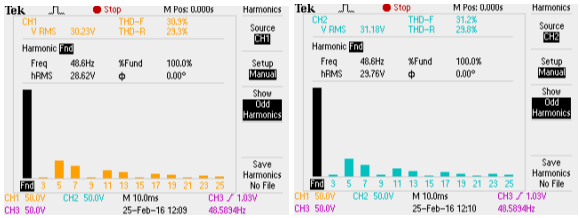

(a) (b)

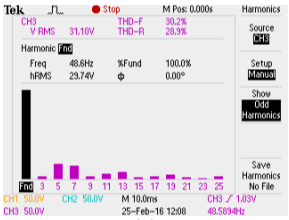

(c)

Fig.19. THD spectrum captured by digital storage oscilloscope (DSO) of phase voltages (a) phase-A, (b) phase-B and (c) phase-C, with BESS in the system.

9. Conclusion

A performance comparison study of grid-tied wind farm without and with BESS is performed through simulation and emulation. The performance

parameters under study were power balance and total harmonic distortion factors. The charge-discharge and discharge-charge transition characteristics of vanadium redox flow batteries is in 'ms' which is justified from the simulation results, which is a feature that can be exploited for its utilization with grid integrated wind energy conversion systems where the response time required is in terms of 'ms' for stable operation of power grid in events like grid side faults and drastic wind variations. From the simulation results, it is proved that the VRFB ESS supports power balance in such events. The total harmonic distortion is also considerably reduced with the use of BESS. The same has been justified through the experimental results also. One large VRFB ESS plant can be installed in the potential 'Wind Farms System Center' and the resource of that VRFB ESS can be utilized by all the wind farms by sequentially switching the cell stacks and varying electrolyte volume for power and energy sharing to mitigate power quality issues. Such a system is proposed as future scope of study.

References

1. Si-Hun Jo, SeoEun Son, Jung-Wook Park: *On Improving Distortion Power Quality Index in Distributed Power Grids.* IEEE Transactions on Smart Grid, Vol. 4, No. 1 (2013), pp.586-595.
2. Cheng-I Chen: *A Calibration Test Platform of Power Quality Instruments for Grid Integration of Wind Energy System*. IEEE Transactions on Industrial Electronics, Vol. 60, No. 7 (2013), pp.2874-2880.
3. Yi Liu, Wenjuan Du, Liye Xiao, Haifeng Wang, Jun Cao: *A Method for Sizing Energy Storage System to Increase Wind Penetration as Limited by Grid Frequency Deviations.* IEEE Transactions on Power Systems, Vol. 31, No. 1 (2016), pp.729-737.
4. Alberto D. Del Rosso, Steven W. Eckroad: *Energy Storage for Relief of Transmission Congestion.* IEEE Transactions on Smart Grid, Vol. 5, No. 2 (2014), pp.1138-1146.
5. Giovanna Oriti, Alexander L. Julian, Nathan J. Peck: *Power-Electronics-Based Energy Management System With Storage.* IEEE Transactions on Power Electronics, Vol. 31, No. 1 (2016), pp.452-460
6. Yun-Su Kim, Eung-Sang Kim, Seung-Il Moon: *Frequency and Voltage Control Strategy of Standalone Microgrids with High Penetration of Intermittent Renewable Generation Systems.* IEEE Transactions on Power Systems, Vol. 31, No. 1 (2016), Pg.718-728.
7. Chua, K.H., Yun Seng Lim, Phil Taylor, Stella Morris, and Jianhui Wong: *Energy Storage System for Mitigating Voltage Unbalance on Low-Voltage Networks With Photovoltaic Systems.* IEEE Transactions on Power Delivery, Vol. 27, No. 4 (2012), pp.1783-1790.
8. Huajie Ding, Pierre Pinson, Zechun Hu, Yonghua Song: *Integrated Bidding and Operating Strategies for Wind-Storage Systems.* IEEE Transactions on Sustainable Energy, Vol. 7, No. 1 (2016), pp.163-172
9. Tsai-Hsiang Chen, Rih-Neng Liao, Chun-Yen Yang, Yen-Hsun Chiang: *Application of Grid-Level Battery Energy Storage System to Wind Power Fluctuation Smoothing.* Journal of Clean Energy Technologies, Vol.4, No.3 (2016)
10. Jha, I.S., Subir Sen, Manish Kr. Tiwari: *Dispatch Control Strategy for Frequency Regulation and Energy Time Shift using Battery Energy Storage Systems.* Power Engineer Journal, Vol.17, No.2 (2015).
11. Tulasichandra Sekhar Gorripotu, Rabindra Kumar Sahu, Sidhartha Panda: *AGC of a multi-area power system under deregulated environment using redox flow batteries and interline power flow controller.* Engineering Science and Technology, an International Journal 18 (2015), pp.555-578.
12. Taesic Kim, Wei Qiao: *A Hybrid Battery Model Capable of Capturing Dynamic Circuit Characteristics and Nonlinear Capacity Effects*. IEEE Transactions on Energy Conversion, Vol. 26, No. 4 (2011) pp.1172-1180.
13. Yang-Wu Shen, De-Ping Ke, Yuan-Zhang Sun, Daniel S. Kirschen, Wei Qiao, Xiang-Tian Deng: *Advanced Auxiliary Control of an Energy Storage Device for Transient Voltage Support of a Doubly Fed Induction Generator.* IEEE Transactions on Sustainable Energy, Vol. 7, No. 1 (2016) pp.63-76.
14. Peng Xiong Chanan Singh: *Optimal Planning of Storage in Power Systems Integrated With Wind Power Generation.* IEEE Transactions on Sustainable Energy, Vol. 7, No. 1 (2016), pp.232-240.
15. Francesco Marra, Guangya Yang, ChrestenTræholt, Jacob Østergaard, Esben Larsen: *A Decentralized Storage Strategy for Residential Feeders with Photovoltaics.* IEEE Transactions on Smart Grid, Vol. 5, No. 2 (2014), pp.974-981.
16. Electropaedia, *Battery and Energy Technologies.* [online] Available: http://www.mpoweruk.com/wind_power.htm (Mar 11, 2017)
17. *CEDRAT*, *2006.* [online] Available: http://www.academia.edu/6071105/PSCAD_Power_System_Simulation (Feb 21, 2017)
18. Prabha Kundur, *Power System stability and Control*, 18th reprint, McGraw Hill Education (India) Private Limited, 2013.
19. Sijia Liu, Jiuchun Jiang, Wei Shi, ZeyuMa, Le Yi Wang, Hongyu Guo: *Butler–Volmer-Equation-Based Electrical Model for High-Power Lithium Titanate Batteries Used in Electric Vehicles.* IEEE Transactions on Industrial Electronics, Vol. 62, No. 12 (2015), pp.7557-7568.

20. Ravishankar Rao Sarma Vrudhula, Daler N.Rakhmatov: *Battery Modeling for Energy-Aware System Design.* Published by the IEEE Computer Society, December 2003
21. Habiballah Rahimi-Eichi, Federico Baronti, Mo-Yuen Chow: *Online Adaptive Parameter Identification and State-of-Charge Coestimation for Lithium-Polymer Battery Cells.* IEEE Transactions on Industrial Electronics, Vol. 61, No. 4 (2014), pp.2053-2061.
22. Khoury, J., Mbayed, R., Salloum, G., Monmasson, E.: *Optimal sizing of a residential PV-battery backup for an intermittent primary energy source under realistic constraints.* Energy and Buildings 105 (2015), pp.206–216.
23. Zhixin Miao, LingXu, Vahid R. Disfani, Lingling Fan: *An SOC-Based Battery Management System for Microgrids.* IEEE Transactions on Smart Grid, Vol. 5, No. 2 (2014), pp.966-973.
24. Mary Jane Shultz, *Engineering Chemistry*, Cengage Learning India Pvt Ltd, New Delhi, 2007
25. David W. Oxtoby, *Modern Chemistry*, Cengage Learning India Pvt Ltd, New Delhi, 2008
26. Xue Feng, Hoay Beng Gooi, Shuaixun Chen: *Capacity fade-based energy management for lithium-ion batteries used in PV systems*. Electric Power Systems Research 129 (2015), pp.150–159.
27. Jia Hongxin, Fu Yang, Zhang Yu, He Weiguo: *Design of Hybrid Energy Storage Control System for Wind Farms Based on Flow Battery and Electric Double-Layer Capacitor.* 978-1-4244-4813-5/10, IEEE, 2010
28. *Draft on Indian Wind Grid Code, 2009*. [online] Available: http://niwe.res.in/NIWE_OLD/Hindi/Docu/Wind_grid_code_for_India%20.pdf (Feb 21, 2017)